DOI: 10.1021/acs.jpca.6b05220

The Absorption Band Shapes of a Push-Pull Dye Approaching the Cyanine Limit: A Challenging Case for First Principle Calculations

Amedeo Capobianco,*,† Raffaele Borrelli,‡ Alessandro Landi,† Amalia Velardo,† and Andrea Peluso*,†

†*Dipartimento di Chimica e Biologia, Università di Salerno, Via G. Paolo II, I-84084 Fisciano (SA), Italy*

‡*Dipartimento di Scienze Agrarie, Forestali e Alimentari, Università di Torino, Largo Paolo Braccini, 2. I-10095 Grugliasco (TO), Italy*

E-mail: acapobianco@unisa.it; apeluso@unisa.it

DOI: 10.1021/acs.jpca.6b05220

Abstract

The absorption band shapes of a solvent tunable donor-acceptor dye have been theoretically investigated by using Kubo's generating function approach, with minimum energy geometries and normal coordinates computed at DFT level of theory. The adopted computational procedure allows to include in the computation of Franck-Condon factors the whole set of normal modes, without any limitation on excitation quanta, allowing for an almost quantitative reproduction of the absorption band-shape when the equilibrium geometries of the ground and the excited states are well predicted by electronic computations. Noteworthy, the functionals which yield more accurate band shapes also provide good prediction of the moment variations upon excitation; since the latter quantities are rarely available, theoretical simulation of band shapes could be a powerful tool for choosing the most appropriate computational method for predictive purposes.

DOI: 10.1021/acs.jpca.6b05220

Introduction

Organic donor-acceptor dyes approaching the cyanine limit, i.e. molecules with a π-conjugated backbone exhibiting vanishing bond length alternation (BLA),[1] have found applications in several technological fields, such as dye-sensitized and bulk-heterojunction solar cells,[2–5] optical storage media,[6,7] and nonlinear optics.[8–11] Highly reliable computational methods are therefore needed for a deeper understanding of their electronic structures and for the rational design of new ones, which should logically include the estimation of the rates of the photochemical processes which occur in devices.[12]

However, the easily polarizable electronic clouds of those compounds make them problematic and challenging systems for most of the computational approaches for large size molecules.[13,14] Time dependent (TD) density functional theory (DFT) predicts vertical excitation energies which significantly disagree with those corresponding to the observed absorption peaks in solution.[15] The discrepancy can be partly ascribed to an insufficient description of double-excitations at TDDFT level,[13,16–18] and partly imputed to nuclear relaxations upon excitation, which makes vertical transitions not corresponding to maximum absorption wavelengths.[19,20] Simulations of the whole absorption band shapes are therefore necessary for better assessing the reliability of electronic computations.[12]

Herein we report first principle calculations of the band shape for the HOMO-LUMO transition of the donor-acceptor (Z)-2-(5-((5-(dibutylamino)thiophen-2-yl)methylene)thiophen-2(5H)-ylidene)malononitrile (**1**) dye, see Scheme 1, which represents a very interesting test case because its absorption spectrum strongly depends on the polarity of the solvent, exhibiting not only a red-shift of the absorption maximum but also a remarkable change of the whole band shape.[21]

By employing a wide palette of DFT approaches, we will show that those functionals which provide a satisfying reproduction of the absorption band shape are the only ones capable of reproducing the observed dipole moment change upon transition. Since the latter quantities are difficult to obtain and are rarely available in the literature,[22] the simulation

DOI: 10.1021/acs.jpca.6b05220

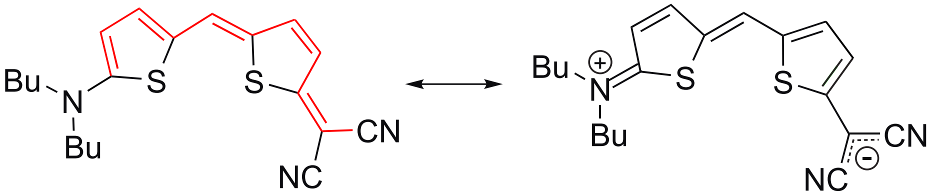

Scheme 1: The neutral (left) and zwitterionic (right) resonance forms of compound **1**. The path used to compute the bond length alternation parameter has been highlighted in red.

of band shapes can represent an alternative feasible way for choosing the most appropriate computational method for a given class of molecules.

Spectral band shapes

According to first order time dependent perturbation theory the absorption cross section per unit time for a radiative transition between the electronic states $|i\rangle$ and $|f\rangle$ is:[23,24]

$$\sigma(\nu) = \frac{8\pi^3\nu}{3nc} I_{fi}(\nu),$$

in which:

$$I_{fi}(\nu) = \sum_l \sum_m |\langle fm| \mu |il\rangle|^2 \, \mathrm{e}^{-\beta E_{il}} \delta(E_{fm} - E_{il} - h\nu)/Z_i \,; \tag{1}$$

c and n stand for the light velocity in vacuum and the index of refraction, μ denotes the dipole moment operator, m and l label the vibrational eigenstates of $|f\rangle$ and $|i\rangle$, respectively, and Z_i is the partition function of the initial state $|i\rangle$. The infinite summations appearing in (1) pose computational problems which, following the seminal works of Lax and Kubo,[23,24] can be conveniently avoided by introducing the integral representation of Dirac's δ function:

$$\delta(E_{fm} - E_{il} - h\nu) = h^{-1} \int_{-\infty}^{\infty} \exp\left[\mathrm{i}\,(E_{fm} - E_{il} - h\nu)\,\tau/\hbar\right] \mathrm{d}\tau \tag{2}$$

writing:

$$I_{fi}(\nu) = h^{-1} \int \mathrm{d}\tau \, \mathrm{e}^{-\mathrm{i}2\pi\nu\tau} I_{fi}(\tau), \tag{3}$$

DOI: 10.1021/acs.jpca.6b05220

with:

$$I_{fi}(\tau) = \mathrm{Tr}\left[\mu_{if}\, \mathrm{e}^{\lambda \mathcal{H}_f} \mu_{fi}\, \mathrm{e}^{-(\beta+\lambda)\mathcal{H}_i}\right], \tag{4}$$

where $\lambda = \mathrm{i}t/\hbar$, $\beta = 1/k_B T$, and $\mathcal{H}_i, \mathcal{H}_f$ are the Hamiltonian operators of the initial and final electronic states, respectively.

The frequency distribution function $I_{fi}(\nu)$, i.e. the spectral band shape, is obtained by the inverse Fourier transform of the function $I_{fi}(\tau)$, where the dummy variable τ has units of time.

If the Hamiltonian operators of the initial and final electronic states are modeled in harmonic approximation, the trace in (4) can be evaluated into a closed form.[24,25] Analytical integration over the vibrational coordinates can be then performed by using Duschinsky's transformation, which allows to express the vibrational coordinates of one electronic state in terms of those of the other:

$$\mathbf{Q}_i = \mathbf{J}\mathbf{Q}_f + \mathbf{K}, \tag{5}$$

where $\mathbf{J}$ is a rotation matrix and $\mathbf{K}$ the vector of the equilibrium position displacements.

The generating function (GF) approach provides several advantages with respect to the standard recursive calculation of Franck-Condon factors,[26–29] inasmuch as it allows to include in computations the whole set of the molecular normal modes, taking into account both the effects due to changes of the equilibrium positions and of vibrational frequencies, as well as the effects due to normal mode mixing. Remarkably, the GF approach does not pose any limitation on the number of modes which can be excited and on their highest quantum numbers. Thus the main limitation consists in neglecting anharmonic effects; in principle they can be included, but the high computational costs pose a limit to the number of vibrational modes which can be treated anharmonically.[30–32] Apart from the use of an apodization function in the fast Fourier transform,[33–35] no external adjustable parameters are needed, so that spectral band shapes obtained by the GF approach ensure an effective test of the performances of the electronic calculations.

DOI: 10.1021/acs.jpca.6b05220

Computational procedure

Absorption spectra were computed by using a local development version of MolFC program.[34,36] The curvilinear coordinate representation of the normal modes has been adopted to prevent that displacements of angular coordinates could result into unrealistic shifts of stretching coordinates upon excitation.[30,37,38] That problem is unavoidable in the rectilinear Cartesian coordinate representation and requires the use of high order anharmonic potentials for its correction.[31,32,39]

The minimum energy geometries of the ground and the first excited states of **1** have been computed at density functional theory level, by using a wide panel of methods, including pure and global hybrid GGA and meta GGA exchange-correlation potentials, see Table 1.

Table 1: Functionals used in the present work.

Functional	Type[a]	% HF exchange[b]	ref
PBE	GGA	0	40
M06-L	mGGA	0	41
B3LYP	GH-GGA	20	42,43
PBE0	GH-GGA	25	44
CAM-B3LYP	RSH-GGA	$19 \xrightarrow{0.33} 65$	45
M06-2X	GH-mGGA	54	41
CAM* [c]	RSH-GGA	$30 \xrightarrow{0.33} 90$	45
ωB97X	RSH-GGA	$16 \xrightarrow{0.30} 100$	46

[a] GGA = generalized gradient approximation, GH = global hybrid, RSH = range-separated hybrid, mGGA = meta-GGA. [b] The percentages of HF exchange in the short (left, α in eq. 6) and long range (right, $\alpha+\beta$ in eq. 6) limits are reported for RSH functionals; the parameter ω (bohr^{-1}) is reported over the arrow. [c] CAM-B3LYP with α and β set to 0.30 and 0.60, respectively.

We have also used range separated hybrid functionals in which the exchange component is divided into short-range (SR) and long-range (LR) terms by splitting the Coulomb operator

DOI: 10.1021/acs.jpca.6b05220

via the error function.[47] Adopting the formalism of ref 45:

$$\frac{1}{r_{12}} = \underbrace{\frac{1 - [\alpha + \beta \operatorname{erf}(\omega r_{12})]}{r_{12}}}_{\mathrm{S}R} + \underbrace{\frac{\alpha + \beta \operatorname{erf}(\omega r_{12})}{r_{12}}}_{\mathrm{L}R}, \tag{6}$$

with $0 \leq \alpha \leq 1, \quad 0 \leq \beta \leq 1, \quad 0 \leq \alpha + \beta \leq 1.$

The DFT exchange interaction is given by the first term of eq. 6, while the long-range orbital-orbital exchange interactions are expressed as Hartree-Fock (HF) exchange integrals. The parameter α is the fraction of HF exchange which contributes over the whole range; the parameter β incorporates the DFT counterpart by a factor of $1 - \alpha - \beta$ and acts in such a way that $\alpha + \beta$ is the fraction of HF exchange in the asymptotic limit; ω defines the range of the separation: the larger its value, the sharper is SR-LR separation. Among long range corrected functionals, we have considered ωB97X which recovers the exact $1/r$ asymptotic behavior of the exchange potential and the 'Coulomb attenuating' CAM-B3LYP functional.[45,46] We have also introduced CAM*, a modification of CAM-B3LYP in which a larger fraction of HF exchange has been imposed by increasing the α and β parameters up to 0.30 and 0.60 respectively, while leaving ω at its default value (0.33 bohr^{-1}), see Table 1.

Effects due to solvent polarization were included by the polarizable continuum model (PCM).[48,49] The non-equilibrium solvation scheme, in which the effects of the slow motion of the solvent are not included, has been used for excited states.[50] The 6-31+G(d,p) basis set was employed for DFT and TDDFT computations because it provides reliable ground and excited state equilibrium geometries and dipole moments.[51–53] Indeed calculations of ground state equilibrium geometries and vertical excitation energies carried out by using the 6-311++G(2df,2p) basis set gave essentially the same results as those obtained by the smaller basis set, see Tables S1-S3 in the Supporting Information.

(PCM)MP2/6-31+G(d) geometry optimizations and computations of ground state dipole moments were also performed to have reference values for the solvents in which electrooptical absorption (EOA) measurements are not available. MP2 was chosen because it is known to

DOI: 10.1021/acs.jpca.6b05220

give reliable dipole moments,[54] even for donor-acceptor systems.[52,53] The Gaussian package was used for MP2, DFT and TDDFT calculations.[55]

Coupled cluster computations including single and approximate double excitations (CC2) in conjunction with the resolution of identity approximation and the aug-cc-pVDZ basis set were carried out by using the TURBOMOLE suite of programs.[56–60] The frozen core approximation was used in MP2 and CC2 computations. The butyl chains of **1** (Scheme 1) have been replaced by methyl groups in all the calculations.

Results

In its most stable *Z* configuration, chromophore **1** can assume the *s-trans* and the *s-cis* conformations shown in Scheme 2.

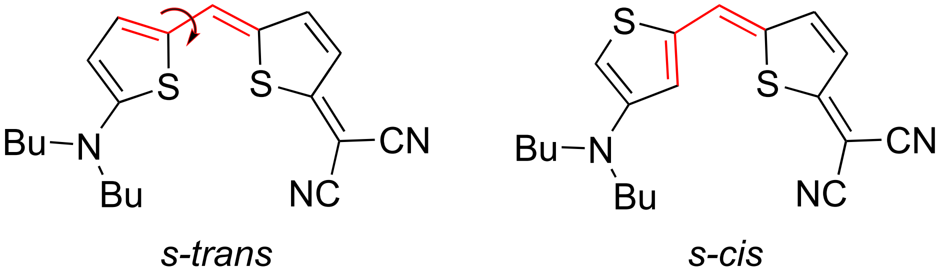

Scheme 2: *s-trans* and *s-cis* conformations of **1**. They differ for the torsion coordinate highlighted in red.

The predicted relative energies are reported in Table 2: *s-trans* conformation is more stable than *s-cis* one according to all the tested methods, in line with ^{1}H-NMR data.[61]

Dipole moments

Experimental and computed ground and excited state dipole moments of **1** are reported in Table 3. Only functionals possessing a high fraction of HF exchange yield dipole moment changes upon excitation ($\Delta\mu = \mu_e - \mu_g$) in reasonable agreement with experimental results. In dioxane, CAM* and ωB97X predict $\Delta\mu$'s of 4.6 and 4.8 D, respectively, in good agreement

DOI: 10.1021/acs.jpca.6b05220

Table 2: Predicted energy differences (kcal/mol) between *s-cis* and *s-trans* conformers of compound 1. DX = 1,4-dioxane, AN = acetonitrile.

	gas	DX	AN
PBE	1.3	1.4	1.5
B3LYP	1.0	1.2	1.4
CAM-B3LYP	0.9	1.1	1.4
M06-2X	1.4	1.6	2.0
CAM*	0.8	1.0	1.5
ωB97X	0.9	1.1	1.6
MP2	1.4	1.5	1.8

with EOA measurements (5 D), whereas pure functionals and functionals with lower fraction of HF exchange, refer to Table 1, yield $\Delta\mu$ as low as 0.1 and ≈1 D, respectively. The localizing effects of HF exchange appear to be crucial for predicting reliable ground state dipole moments, high-exchange functionals approaching the accuracy of MP2.[52,53,62] Indeed, upon increasing the fraction of HF exchange in the functional, ground state dipole moments decrease whereas excited state ones increase, leading to a significant increase of $\Delta\mu$'s.

Absorption band shapes

In non-polar solvents, the UV/vis absorption spectrum of compound **1** is characterized by two well resolved peaks, falling in 1,4-dioxane at 15385 and 16491 cm^{-1} and possessing roughly the same intensity, see Figure 1.[21] As the solvent polarity increases, the longer wavelength absorption gains intensity and shifts to lower frequencies (ca 15110 cm^{-1} in acetonitrile, Figure 1, orange line), whereas the shorter wavelength peak becomes a shoulder.

Since absorption spectra are known to exhibit only a marginal dependence on conformational degrees of freedom, we have first focused attention on the most stable *s-trans* conformer, c.f. Table 2. The computed absorption spectra at $T = 298$ K in low polar environment (1,4-dioxane) are reported in Figure 2, together with the experimental spectrum (dashed line). Intensities have been scaled in such a way that all the spectra possess the same area. For a proper comparison of band-shapes, spectra have been aligned by letting the computed and the experimental wavenumbers of the minimum absorption between the

Table 3: Computed and experimental ground (μ_g) and excited state (μ_e)[a] dipole moments (D). DX = 1,4-dioxane, AN = acetonitrile. Computations refer to *s-trans* conformation.

	gas		DX		AN	
	μ_g	μ_e	μ_g	μ_e	μ_g	μ_e
PBE	14.6	15.0	18.5	18.6	24.4	23.6
M06-L	14.4	14.9	18.2	18.3	23.8	23.0
B3LYP	14.4	15.5	18.2	19.1	24.4	23.9
PBE0	14.2	15.5	18.0	19.0	24.2	23.6
CAM-B3LYP	13.3	16.3	16.9	19.9	23.9	24.1
M06-2X	12.7	16.0	16.2	19.6	22.7	23.7
CAM*	12.6	16.6	15.7	20.3	22.8	24.5
ωB97X	12.4	16.4	15.5	20.3	22.9	24.5
MP2	11.1	–	13.6	–	19.1	–
exper	*11.2*	*16.7*	*14.0*	*19.0*	–	–

[a] Vertical approximation, see ref 22. [b] Ref 21; gas phase values were obtained by using the Onsager model, see ref 61.

two peaks coincide, but for a) of Figure 2 where the alignment has been done on the longer wavelength peak. Panel a) of Figure 2 shows that pure functionals as well as functionals with low fraction of HF exchange are not able to reproduce the essential features of the experimental spectrum. The predicted band shapes exhibit only one peak instead of two, with a small shoulder at shorter wavelength. Furthermore, the predicted bandwidths are significantly narrower than the experimental one.

The agreement between observed and predicted band shapes improves significantly by employing equilibrium geometries and normal modes predicted by functionals with higher fraction of HF exchange. Figure 2b shows that CAM-B3LYP yields in 1,4-dioxane two well resolved peaks, whose intensity ratio is however significantly different from the observed (1:1) one. Further improvement is obtained by increasing the amount of Hartree-Fock exchange in the functional: the CAM*, our modification of CAM-B3LYP discussed above, see Table 1, yields an absorption band shape characterized by two peaks with intensity ratio 1.2:1, in satisfying agreement with the experimental one, see Figure 2c. The energy difference between the two absorption peaks is slightly overestimated (1430 vs ≈1100 cm^{-1}) and the

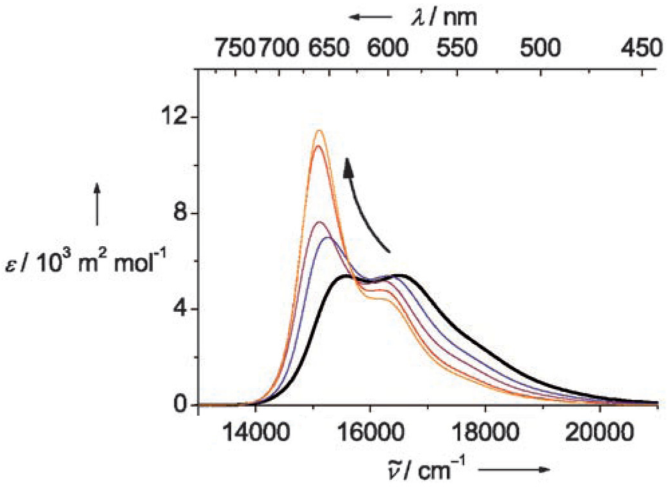

Figure 1: UV/Vis absorption spectra of dye **1** in solvents of different polarity at 298 K ($c = 10^{-5}$ M). The thick black line is for the least polar solvent diethyl ether (in 1,4-dioxane the spectra is almost identical), blue line: ethyl acetate, purple line: tetrahydrofuran, red line: acetone, and orange line: acetonitrile. The arrow indicates the spectral shift with increasing solvent polarity. Reproduced with permission from ref 21. Copyright (2008) John Wiley and Sons.

simulated spectrum is slightly broader than the observed one. Those small discrepancies can be attributed to anharmonic effects, which can be simply corrected –without affecting peak intensity ratios– by using standard scaling factors for the computed vibrational frequencies,[63] see Figure S1 in the Supporting Information.

The intensity ratio between the two absorption peaks approaches the observed 1:1 value by using predicted CAM* geometries and normal modes in the gas-phase, Figure 2d, suggesting that solvent polarization effects modeled by PCM could be slightly overestimated.[19] M06-2X and ωB97X functionals give band shapes very similar to that obtained by CAM-B3LYP and CAM*, respectively (see Figures S1-S4 in the Supporting Information), thus showing that the amount of exact exchange is the key factor to achieve a good accuracy for the vibronic spectra of compound **1**.

In weakly polar environments *s-cis* is predicted to be less stable than *s-trans* conformer by ca 1 kcal/mol according to CAM* and ωB97X functionals (Table 2). Given that exiguous energy difference, close to calculation accuracy, it is possible that *s-cis* is sufficiently populated to be detected at room temperature. We have therefore also computed the spectrum

DOI: 10.1021/acs.jpca.6b05220

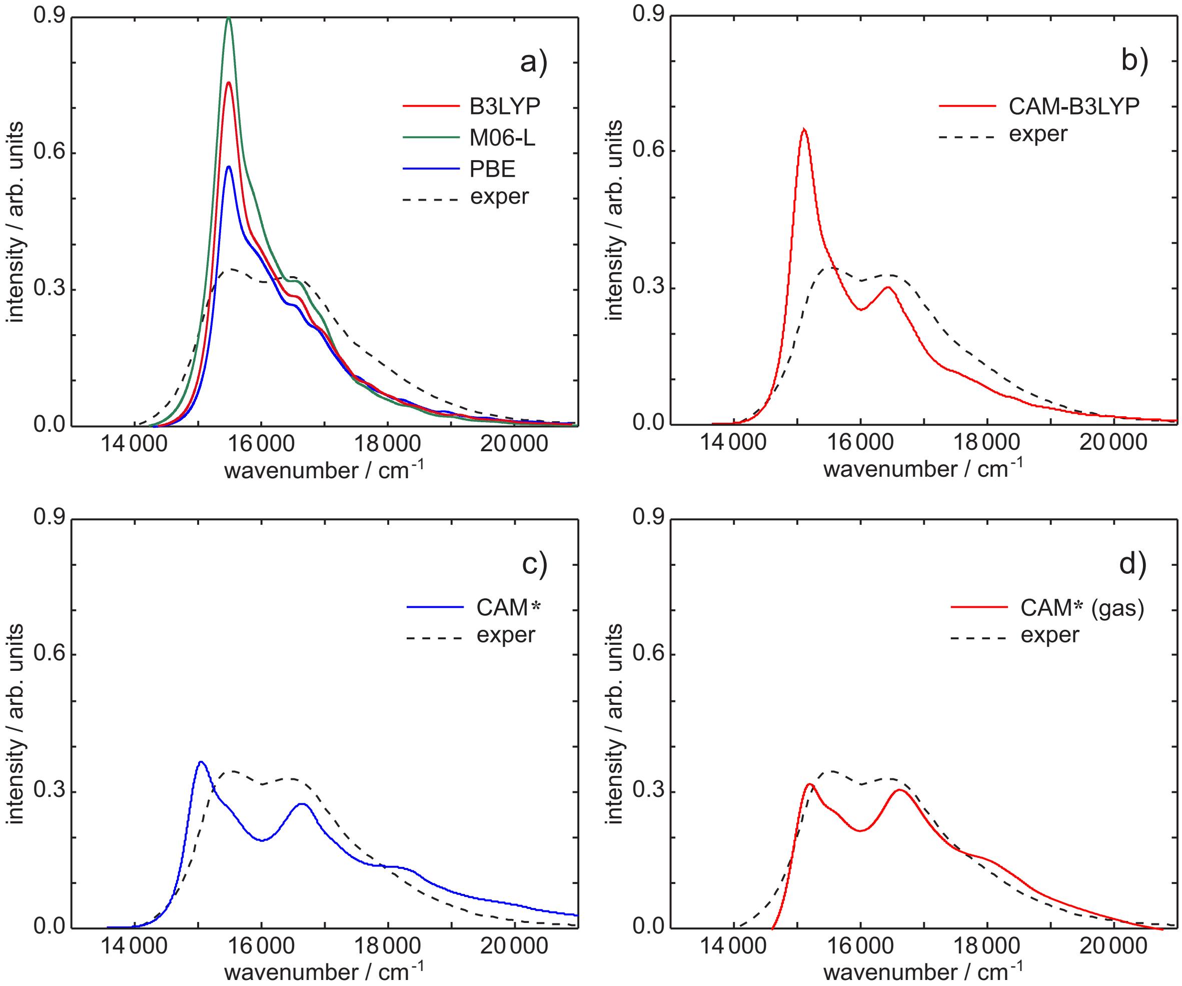

Figure 2: Predicted UV/absorption spectra of **1** (*s-trans* conformer) in dioxane (panels a-c) and in the gas phase (panel d) at $T = 298$ K. The experimental spectrum has been superimposed as a dashed line.

of that conformer in low polar environments (gas and dioxane) by using the best performing functionals (CAM* and ωB97X). Figure 3 reports the gas-phase spectra obtained at the CAM* level for *s-trans* and *s-cis* conformers. As expected, both conformers exhibit very similar spectra, at variance with **1**/*s-trans*, the **1**/*s-cis* conformer exhibits the shorter wavelength peak slightly more intense than the longer wavelength one. The same also holds in 1,4-dioxane, see Figure S3 in the Supporting Information.

Computed ($T = 298$ K) and experimental absorption spectra in acetonitrile are reported in Figure 4. They have been aligned by making coincident the wavenumber of the absorption maximum; intensities have been properly normalized, so that all the spectra possess the same

DOI: 10.1021/acs.jpca.6b05220

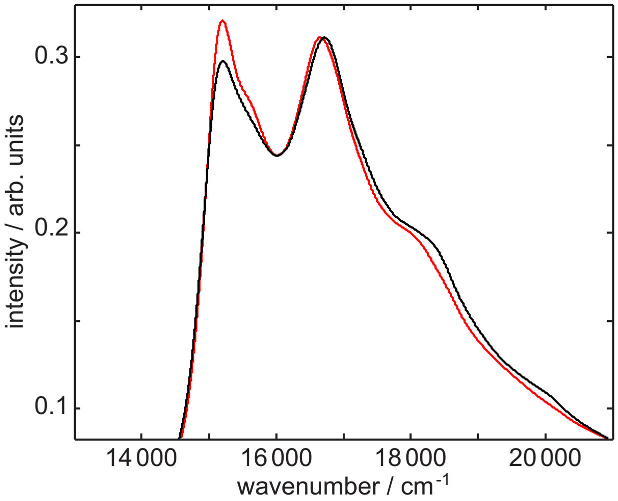

Figure 3: Predicted (CAM*, gas) UV/absorption spectra of **1**, *s-trans* conformer, red line; *s-cis* conformer, black line.

area. As the polarity of solvent increases, bandwidths are predicted to be narrower and less structured than those obtained in low polar solvents (compare with Figure 2), in line with experimental results.

With the exception of PBE, all the functionals yield a reasonably accurate spectrum, but still high-exchange functionals (Figure 4, panels c and d) ensure the best agreement with the experiment.

The assignments of the two peaks in low polar solvents are not a simple matter because, apart from one low frequency mode which is significantly more displaced than all the others, there is a huge number (30-40) of slightly displaced modes. The components of the equilibrium position displacement vector **K** predicted by two prototypical functionals, B3LYP and CAM*, in the gas-phase and in acetonitrile, are reported in Table 6. In both environments and according to both functionals, the most displaced vibrational coordinate is an in plane low frequency bending mode, which involves the whole molecular backbone. The frequency of that mode is too low for being responsible of the two peaks observed in low polar environments. At room temperature that mode plays an important role, inasmuch as it broadens the absorption bands by providing vibronic progressions which, because hot vibronic states are populated, fall around the most intense transitions, both at shorter and longer wave-

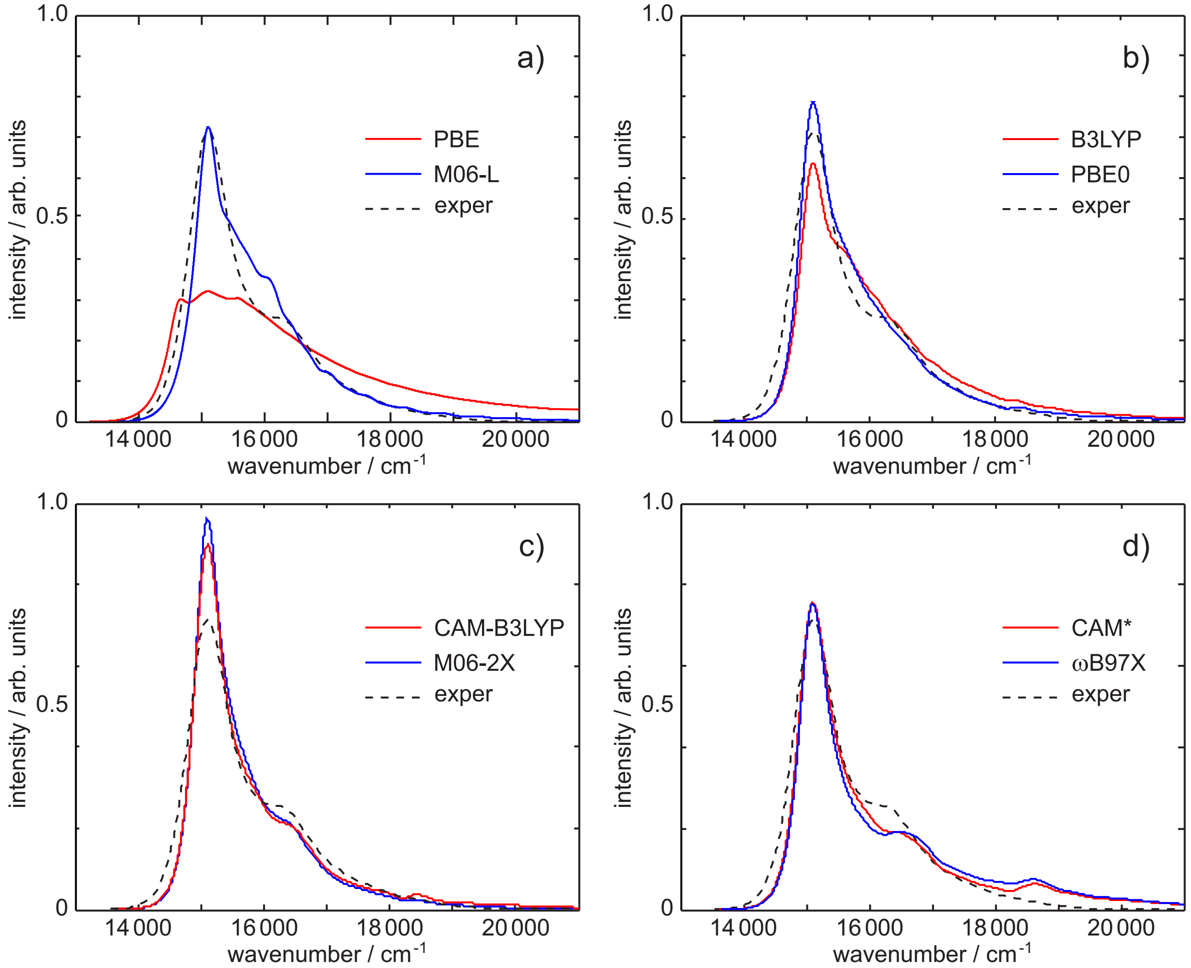

Figure 4: Predicted and observed (dashed line) UV/absorption spectra of **1** in acetonitrile at 298 K.

lengths. As concerns the higher frequencies, the comparison between the **K** components predicted by B3LYP and CAM* indicates that the most significant differences are found in the region 1500-1600 cm^{-1}, where CAM* predict three modes, whose equilibrium position displacements are significantly large, see Table 6, whereas no displaced modes are predicted by B3LYP in that wavenumber region. The computed CAM* and B3LYP spectra of **1** at 0 K, obtained by using the usual recursive FC calculation, are displayed in Figure 5. Only the first ten most displaced vibrational modes are allowed to change their quantum number upon electronic transition in those computations. While the B3LYP spectrum extends up to 1400 cm^{-1}, showing only two major absorption regions, one in the range 0-500 cm^{-1}, the other extending from 1000 to 1300 cm^{-1}, the CAM* spectrum exhibits a third absorption region, from 1500 up to 1800 cm^{-1}. In that region at least three vibronic progressions can be distinguished, involving 0←1 transition of the displaced modes at $\tilde{\nu} = 1521, 1574, 1601$ cm^{-1}, accompanied by several $0 \leftarrow n$ transitions of the most displaced low frequency mode, with n from 1 at least to 5, the maximum excitation number used in computations. The density of states provided by those transitions is significantly higher than that computed at 1000-1300 cm^{-1}, giving rise to the second peak at shorter wavelength appearing in low polar solvents. The three displaced modes predicted by CAM* at $\tilde{\nu} = 1521, 1574, 1601$ cm^{-1} correspond to stretching and bending vibrations of the whole molecular skeleton.

The comparison of the insets of Figure 5, computed by GF approach at $T = 4$ K and including excitation of all normal modes, with figures 2-4, obtained at $T = 298$ K, shed light on the important role played by the large number of low frequency displaced modes of Table 6. These modes provide hot transitions which significantly broaden the few vibronic $\vec{n} \leftarrow 0$ transitions computed at 0 K. It is interesting to observe how molecular modes are able to provide by themselves bandwidths which compare well with their experimental counterparts.[64]

In acetonitrile, CAM* computations predict that only one high frequency mode (1694 cm^{-1}) is displaced. Although the displacement is significant (≈ 0.4) a single displaced mode is not sufficient to provide a high density of states in that region, so that the second peak disappears and the whole spectrum becomes narrower.

Because of the high number of displaced modes, it could be useful to try to relate the absorption band shapes to some sort of collective coordinate, such as the bond length alternation (BLA) or the bond order alternation (BOA). BLA is defined as the difference between the average lengths of the nominally single and double bonds along a π-conjugated backbone; it is an important physicochemical parameter for understanding the electronic properties of dyes, which, together with the bond order alternation, has proven particularly useful in designing organic materials with high nonlinear optical properties.[65] Here, we will consider

DOI: 10.1021/acs.jpca.6b05220

only BLA, since absorption band shapes are more directly related to molecular geometry changes.

Computed BLA are reported in Table 4. For all the environments, ground state BLA's increases upon increasing the fraction of exact exchange in the functional,[66,67] as seen e.g. by B3LYP and CAM* estimates in dioxane, amounting to 0.02 and 0.05 Å, respectively. Noteworthy, only functionals giving BLA $\geq 5 \times 10^{-2}$ Å at the ground state are capable of reproducing both the observed $\Delta\mu$ and the absorption band shape in low-polarity environments. As already noted, both ground and excited state dipole moments increase upon increasing the polarity of the solvent, but μ_g increases at a larger extent, causing a lowering of $\Delta\mu$ (see Table 3). That happens because the excited state is strongly polarized already in the gas phase, as shown by the BLA's of excited states reported in Table 4.

Table 4: Predicted ground (gr) and excited (ex) state BLA (10^{-2} **Å**)**.**

	GAS		DX		AN	
	gr	ex	gr	ex	gr	ex
PBE	2	−1	2	−2	0	−2
M06-L	3	−1	2	−2	0	−2
B3LYP	4	0	2	−1	0	−2
PBE0	4	0	2	−1	0	−2
CAM-B3LYP	5	0	4	0	0	0
M06-2X	5	1	4	0	0	0
CAM*	6	0	5	0	2	0
ωB97X	6	0	5	0	2	0

Absorption energies

Table 5 shows that vertical transition energies are systematically overestimated with respect to experimental maximum absorption energies; the poor performance on the prediction of reliable excitation energies for cyanines is a well documented issue, which is known to affect the quality of almost all the computational methods, not only TDDFT.[68] Noteworthy, our calculations have shown that maximum absorptions occurs, within 0.01 eV (80 cm^{-1}), at the energy of the $0 \leftarrow 0$ transition rather than at that corresponding to the vertical one. The

DOI: 10.1021/acs.jpca.6b05220

energy differences between the vertical transition and the $0 \leftarrow 0$ one can be as large as 0.24 eV, see Table 5, so that the computation of vibronic band shapes appears a necessary task to make a meaningful comparison of experimental and predicted transition energies. Indeed, a better agreement between theoretical and experimental transition energies is obtained by correctly comparing computed and experimental maximum absorption energies,[13,20,69] see Table 5. Notwithstanding, predicted transition energies are still significantly overestimated; interestingly pure functionals or functional with a low ratio of HF exchange yield transition energies in better agreement with experimental ones, even though they fail in predicting the real electronic structure of **1**.

For the specific case under investigation, we have found that reliable transition energies can be obtained by using single point CC2 calculations with the minimum energy geometries obtained by functionals which better reproduce band shapes and estimating solvent polarization effects from DFT computations. Adopting the minimum energy geometries from ωB97X optimizations of the ground and the first excited state, the electronic transition in the gas-phase is predicted at 2.21 eV by CC2 computations. Since the ground and excited state dipole moments predicted at CC2 level (12.3 and 18.5 D, respectively) are very similar to those obtained by the ωB97X functional (see Table 3), the effect of solvent polarization can be safely taken from DFT computations ($\approx$ 0.27 eV in going from the gas-phase to 1,4-dioxane), or estimated by the Onsager model. Using the former choice and neglecting zero point vibrational energy changes upon transition, we obtained $E_{00} = 1.94$ eV, in pretty good agreement with the experimental spectrum (1.92 eV).

Conclusions

Donor-acceptor dyes possessing easily polarizable electronic clouds are difficult systems for DFT computations. Methods based on pure or low percentage of HF exchange functionals yield excitation energies more close to the experimental ones, but they erroneously assign a

DOI: 10.1021/acs.jpca.6b05220

Table 5: Predicted maximum absorption (E_m), vertical (E_v) and E_{00} transition energies. All data are expressed in eV.

	gas			DX			AN		
	E_m	E_{00}	E_v	E_m	E_{00}	E_v	E_m	E_{00}	E_v
PBE	2.20	2.21	2.36	2.03	2.03	2.17	2.10	2.05	2.20
M06-L	2.34	2.25	2.50	2.17	2.17	2.31	2.17	2.19	2.33
B3LYP	2.36	2.38	2.53	2.17	2.17	2.31	2.19	2.19	2.32
PBE0	2.42	2.43	2.58	2.22	2.22	2.36	2.24	2.24	2.37
CAM-B3LYP	2.52	2.53	2.73	2.27	2.28	2.45	2.29	2.29	2.38
M06-2X	2.50	2.51	2.70	2.25	2.26	2.42	2.25	2.25	2.34
CAM*	2.66	2.66	2.95	2.39	2.39	2.63	2.38	2.39	2.46
ωB97X	2.60	2.60	2.88	2.33	2.32	2.56	2.31	2.32	2.38
exper.	–	–	–	*1.92*	–	–	*1.87*	–	–

cyanine-like character to chromophore **1** in low polar solvents, predicting a dipole moment change upon electronic transitions which is largely underestimated with respect to the results of EOA measurements. Instead, functionals with high percentage of HF exchange correctly reproduce the dipole moment variation upon excitation and provide reliable absorption band shapes. Since EOA measurements are scarce in the literature and difficult to obtain in highly polar solvents, band-shape computations can be an alternative reliable criterion for choosing the best computational tool for difficult cases as that considered here. It is also a necessary effort for a meaningful comparison between computed and observed excitation energies.

Acknowledgement

The financial supports of PON2007-2014 (Relight project) and of the University of Salerno are gratefully acknowledged.

Supporting Information Available

Dipole moments and excitation energies evaluated by using the 6-311++G(2df,2p) basis set (Tables S1-S3). Spectra not shown in the article (Figures S1-S4). Plots of HOMO and LUMO, Figure S5. This material is available free of charge via the Internet at `http://pubs.acs.org/`.

DOI: 10.1021/acs.jpca.6b05220

References

(1) Tolbert, L. M.; Zhao, X. Beyond the Cyanine Limit: Peierls Distortion and Symmetry Collapse in a Polymethine Dye. *J. Am. Chem. Soc.* **1997**, *119*, 3253–3258.

(2) Tatay, S.; Haque, S. A.; O'Regan, B.; Durrant, J. R.; Verhees, W. J. H.; Kroon, J. M.; Vidal-Ferran, A.; Gaviña, P.; Palomares, E. Kinetic Competition in Liquid Electrolyte and Solid-State Cyanine Dye Sensitized Solar Cells. *J. Mater. Chem.* **2007**, *17*, 3037.

(3) Bürckstümmer, H.; Tulyakova, E. V.; Deppisch, M.; Lenze, M. R.; Kronenberg, N. M.; Gsänger, M.; Stolte, M.; Meerholz, K.; Würthner, F. Efficient Solution-Processed Bulk Heterojunction Solar Cells by Antiparallel Supramolecular Arrangement of Dipolar Donor-Acceptor Dyes. *Angew. Chem. Int. Ed.* **2011**, *50*, 11628–11632.

(4) Borrelli, R.; Ellena, S.; Barolo, C. Theoretical and Experimental Determination of the Absorption and Emission Spectra of a Prototypical Indolenine-Based Squaraine Dye. *Phys. Chem. Chem. Phys.* **2014**, *16*, 2390–2398.

(5) Park, J.; Barbero, N.; Yoon, J.; Dell'Orto, E.; Galliano, S.; Borrelli, R.; Yum, J.-H.; Censo, D. D.; Grätzel, M.; Nazeeruddin, M. K. et al. Panchromatic Symmetrical Squaraines: A Step Forward in the Molecular Engineering of Low Cost Blue-Greenish Sensitizers for Dye-Sensitized Solar Cells. *Phys. Chem. Chem. Phys.* **2014**, *16*, 24173–24177.

(6) Mustroph, H.; Stollenwerk, M.; Bressau, V. Current Developments in Optical Data Storage with Organic Dyes. *Angew. Chem. Int. Ed.* **2006**, *45*, 2016–2035.

(7) Klajn, R. Spiropyran-Based Dynamic Materials. *Chem. Soc. Rev.* **2014**, *43*, 148–184.

(8) Dalton, L. R.; Sullivan, P. A.; Bale, D. H. Electric Field Poled Organic Electro-Optic Materials: State of the Art and Future Prospects. *Chem. Rev.* **2010**, *110*, 25–55.

(9) Kang, H.; Facchetti, A.; Jiang, H.; Cariati, E.; Righetto, S.; Ugo, R.; Zuccaccia, C.; Macchioni, A.; Stern, C. L.; Liu, Z. et al. Ultralarge Hyperpolarizability Twisted π-Electron System

Electro-Optic Chromophores: Synthesis, Solid-State and Solution-Phase Structural Characteristics, Electronic Structures, Linear and Nonlinear Optical Properties, and Computational Studies. *J. Am. Chem. Soc.* **2007**, *129*, 3267–3286.

(10) Castaldo, A.; Centore, R.; Peluso, A.; Sirigu, A.; Tuzi, A. Structure and Electronic Properties of Extended Chromophores for Applications in Second-Order Nonlinear Optics. *Struct. Chem.* **2002**, *13*, 27–36.

(11) Hu, H.; Fishman, D. A.; Gerasov, A. O.; Przhonska, O. V.; Webster, S.; Padilha, L. A.; Peceli, D.; Shandura, M.; Kovtun, Y. P.; Kachkovski, A. D. et al. Two-Photon Absorption Spectrum of a Single Crystal Cyanine-like Dye. *J. Phys. Chem. Lett.* **2012**, *3*, 1222–1228.

(12) Velardo, A.; Borrelli, R.; Capobianco, A.; La Rocca, M. V.; Peluso, A. First Principle Analysis of Charge Dissociation and Charge Recombination Processes in Organic Solar Cells. *J. Phys. Chem. C* **2015**, *119*, 18870–18876.

(13) Send, R.; Valsson, O.; Filippi, C. Electronic Excitations of Simple Cyanine Dyes: Reconciling Density Functional and Wave Function Methods. *J. Chem. Theory Comput.* **2011**, *7*, 444–455.

(14) Zhekova, H.; Krykunov, M.; Autschbach, J.; Ziegler, T. Applications of Time Dependent and Time Independent Density Functional Theory to the First π to π^* Transition in Cyanine Dyes. *J. Chem. Theory Comput.* **2014**, *10*, 3299–3307.

(15) Jacquemin, D.; Perpète, E. A.; Ciofini, I.; Adamo, C.; Valero, R.; Zhao, Y.; Truhlar, D. G. On the Performances of the M06 Family of Density Functionals for Electronic Excitation Energies. *J. Chem. Theory Comput.* **2010**, *6*, 2071–2085.

(16) Masunov, A. E. Theoretical Spectroscopy of Carbocyanine Dyes Made Accurate by Frozen Density Correction to Excitation Energies Obtained by TD-DFT. *Int. J. Quantum Chem.* **2010**, *110*, 3095–3100.

(17) Grimme, S.; Neese, F. Double-Hybrid Density Functional Theory for Excited Electronic States of Molecules. *J. Chem. Phys.* **2007**, *127*, 154116.

(18) Moore II, B.; Autschbach, J. Longest-Wavelength Electronic Excitations of Linear Cyanines: The Role of Electron Delocalization and of Approximations in Time-Dependent Density Functional Theory. *J. Chem. Theory Comput.* **2013**, *9*, 4991–5003.

(19) Jacquemin, D.; Chibani, S.; Le Guennic, B.; Mennucci, B. Solvent Effects on Cyanine Derivatives: A PCM Investigation. *J. Phys. Chem. A* **2014**, *118*, 5343–5348.

(20) Avila Ferrer, F. J.; Cerezo, J.; Stendardo, E.; Improta, R.; Santoro, F. Insights for an Accurate Comparison of Computational Data to Experimental Absorption and Emission Spectra: Beyond the Vertical Transition Approximation. *J. Chem. Theory Comput.* **2013**, *9*, 2072–2082.

(21) Würthner, F.; Archetti, G.; Schmidt, R.; Kuball, H.-G. Solvent Effect on Color, Band Shape, and Charge-Density Distribution for Merocyanine Dyes Close to the Cyanine Limit. *Angew. Chem. Int. Ed.* **2008**, *47*, 4529–4532.

(22) Liptay, W. Electrochromism and Solvatochromism. *Angew. Chem. Int. Ed.* **1969**, *8*, 177–188.

(23) Lax, M. The Franck-Condon Principle and Its Application to Crystals. *J. Chem. Phys.* **1952**, *20*, 1752–1760.

(24) Kubo, R.; Toyozawa, Y. Application of the Method of Generating Function to Radiative and Non-Radiative Transitions of a Trapped Electron in a Crystal. *Prog. Theor. Phys.* **1955**, *13*, 160–182.

(25) Husimi, K. Some Formal Properties of the Density Matrix . *Proc. Phys. Math. Soc. Japan* **1940**, *22*, 264–314.

(26) Doktorov, E. V.; Malkin, I. A.; Man'ko, V. I. Dynamical Symmetry of Vibronic Transitions in Polyatomic Molecules and the Franck-Condon Principle. *J. Mol. Spectrosc.* **1977**, *64*, 302–326.

(27) Peluso, A.; Santoro, F.; Del Re, G. Vibronic Coupling in Electronic Transitions with Significant Duschinsky Effect. *Int. J. Quant. Chem.* **1997**, *63*, 233–244.

(28) Borrelli, R.; Peluso, A. Dynamics of Radiationless Transitions in Large Molecular Systems: A Franck-Condon Based Method Accounting for Displacements and Rotations of All the Normal Coordinates. *J. Chem. Phys.* **2003**, *119*, 8437–8448.

(29) Santoro, F.; Lami, A.; Improta, R.; Bloimo, J.; Barone, V. Effective method for the computation of optical spectra of large molecules at finite temperature including the Duschinsky and Herzberg-Teller effect: The band of porphyrin as a case study. *J. Chem. Phys.* **2008**, *128*, 224311.

(30) Capobianco, A.; Borrelli, R.; Noce, C.; Peluso, A. Franck-Condon Factors in Curvilinear Coordinates: The Photoelectron Spectrum of Ammonia. *Theor. Chem. Acc.* **2012**, *131*, 1181.

(31) Peluso, A.; Borrelli, R.; Capobianco, A. Photoelectron Spectrum of Ammonia, a Test Case for the Calculation of Franck–Condon Factors in Molecules Undergoing Large Geometrical Displacements upon Photoionization. *J. Phys. Chem. A* **2009**, *113*, 14831–14837.

(32) Peluso, A.; Borrelli, R.; Capobianco, A. Correction to “Photoelectron Spectrum of Ammonia, a Test Case for the Calculation of Franck-Condon Factors in Molecules Undergoing Large Geometrical Displacements upon Photoionization”. *J. Phys. Chem. A* **2013**, *117*, 10985–10985.

(33) Borrelli, R.; Capobianco, A.; Peluso, A. Generating Function Approach to the Calculation of Spectral Band Shapes of Free-Base Chlorin Including Duschinsky and Herzberg-Teller Effects. *J. Phys. Chem. A* **2012**, *116*, 9934–9940.

(34) Borrelli, R.; Capobianco, A.; Peluso, A. Franck-Condon Factors: Computational Approaches and Recent Developments. *Can. J. Chem.* **2013**, *91*, 495–504.

(35) Borrelli, R.; Peluso, A. The Temperature Dependence of Radiationless Transition Rates from Ab Initio Computations. *Phys. Chem. Chem. Phys.* **2011**, *13*, 4420–4426.

(36) Borrelli, R.; Peluso, A. MolFC: A program for Franck-Condon integrals calculation. Package available online at `http://www.theochem.unisa.it`.

(37) Borrelli, R.; Peluso, A. The Vibrational Progressions of the N ← V Electronic Transition of Ethylene. A Test Case for the Computation of Franck-Condon Factors of Highly Flexible Photoexcited Molecules. *J. Chem. Phys.* **2006**, *125*, 194308–8.

(38) Borrelli, R.; Peluso, A. Erratum: "The Vibrational Progressions of the N ← V Electronic Transition of Ethylene: A Test Case for the Computation of Franck-Condon Factors of Highly Flexible Photoexcited Molecules". *J. Chem. Phys.* **2013**, *139*, 159902–1.

(39) Hoy, A. R.; Mills, I. M.; Strey, G. Anharmonic Force Constant Calculations. *Mol. Phys.* **1972**, *24*, 1265–1290.

(40) Perdew, J. P.; Burke, K.; Ernzerhof, M. Generalized Gradient Approximation Made Simple. *Phys. Rev. Lett.* **1996**, *77*, 3865–3868.

(41) Zhao, Y.; Truhlar, D. G. The M06 Suite of Density Functionals for Main Group Thermochemistry, Thermochemical Kinetics, Noncovalent Interactions, Excited States, and Transition Elements: Two New Functionals and Systematic Testing of Four M06-class Functionals and 12 Other Functionals. *Theor. Chem. Acc.* **2007**, *120*, 215–241.

(42) Becke, A. D. Density-Functional Thermochemistry. III. The Role of Exact Exchange. *J. Chem. Phys.* **1993**, *98*, 5648–5652.

(43) Stephens, P. J.; Devlin, F. J.; Chabalowski, C. F.; Frisch, M. J. Ab Initio Calculation of Vibrational Absorption and Circular Dichroism Spectra Using Density Functional Force Fields. *J. Phys. Chem.* **1994**, *98*, 11623–11627.

(44) Perdew, J. P.; Ernzerhof, M.; Burke, K. Rationale for Mixing Exact Exchange with Density Functional Approximations. *J. Chem. Phys.* **1996**, *105*, 9982–9985.

(45) Yanai, T.; Tew, D. P.; Handy, N. C. A New Hybrid Exchange-Correlation Functional Using the Coulomb-Attenuating Method (CAM-B3LYP). *Chem. Phys. Lett.* **2004**, *393*, 51–57.

(46) Chai, J.-D.; Head-Gordon, M. Systematic Optimization of Long-Range Corrected Hybrid Density Functionals. *J. Chem. Phys.* **2008**, *128*, 084106–15.

DOI: 10.1021/acs.jpca.6b05220

(47) Iikura, H.; Tsuneda, T.; Yanai, T.; Hirao, K. A Long-Range Correction Scheme for Generalized-Gradient-Approximation Exchange Functionals. *J. Chem. Phys.* **2001**, *115*, 3540–3544.

(48) Miertuš, S.; Scrocco, E.; Tomasi, J. Electrostatic Interaction of a Solute with a Continuum. A Direct Utilization of Ab Initio Molecular Potentials for the Prevision of Solvent Effects. *Chem. Phys.* **1981**, *55*, 117–129.

(49) Tomasi, J.; Mennucci, B.; Cammi, R. Quantum Mechanical Continuum Solvation Models. *Chem. Rev.* **2005**, *105*, 2999–3094.

(50) Barone, V.; Ferretti, A.; Pino, I. Absorption Spectra of Natural Pigments as Sensitizers in Solar Cells by TD-DFT and MRPT2: Protonated Cyanidin. *Phys. Chem. Chem. Phys.* **2012**, *14*, 16130–16137.

(51) Charaf-Eddin, A.; Planchat, A.; Mennucci, B.; Adamo, C.; Jacquemin, D. Choosing a Functional for Computing Absorption and Fluorescence Band Shapes with TD-DFT. *J. Chem. Theory Comput.* **2013**, *9*, 2749–2760.

(52) Capobianco, A.; Centore, R.; Noce, C.; Peluso, A. Molecular Hyperpolarizabilities of Push-Pull Chromophores: A Comparison between Theoretical and Experimental Results. *Chem. Phys.* **2013**, *411*, 11–16.

(53) Capobianco, A.; Centore, R.; Fusco, S.; Peluso, A. Electro–Optical Properties from CC2 Calculations: A Comparison between Theoretical and Experimental Results. *Chem. Phys. Lett.* **2013**, *580*, 126–129.

(54) Hellweg, A. The Accuracy of Dipole Moments from Spin-Component Scaled CC2 in Ground and Electronically Excited Dipole Moments. *J. Chem. Phys.* **2011**, *133*, 064103–9.

(55) Frisch, M. J.; Trucks, G. W.; Schlegel, H. B.; *et al*, Gaussian 09 Revision D.01. Gaussian Inc. Wallingford CT 2009.

(56) Christiansen, O.; Koch, H.; Jørgensen, P. The Second-Order Approximate Coupled Cluster Singles and Doubles Model CC2. *Chem. Phys. Lett.* **1995**, *243*, 409–418.

(57) Hättig, C.; Weigend, F. CC2 Excitation Energy Calculations on Large Molecules Using the Resolution of the Identity Approximation. *J. Chem. Phys.* **2000**, *113*, 5154–5161.

(58) Dunning, T. H. Gaussian Basis sets for Use in Correlated Molecular Calculations. I. The Atoms Boron through Neon and Hydrogen. *J. Chem. Phys.* **1989**, *90*, 1007–1023.

(59) Weigend, F.; Köhn, A.; Hättig, C. Efficient Use of the Correlation Consistent Basis Sets in Resolution of the Identity MP2 Calculations. *J. Chem. Phys.* **2002**, *116*, 3175–3183.

(60) TURBOMOLE V6.3.1 2011, a development of University of Karlsruhe and Forschungszentrum Karlsruhe GmbH, 1989-2007, TURBOMOLE GmbH, since 2007; available from `http://www.turbomole.com`.

(61) Würthner, F.; Thalacker, C.; Matschiner, R.; Lukaszuk, K.; Wortmann, R. Optimization of Neutrocyanine Chromophores Based on Five-membered Heterocycles for Photorefractive Applications. *Chem. Commun.* **1998**, 1739–1740.

(62) Centore, R.; Fusco, S.; Peluso, A.; Capobianco, A.; Stolte, M.; Archetti, G.; Kuball, H.-G. Push-Pull Azo-Chromophores Containing Two Fused Pentatomic Heterocycles and Their Nonlinear Optical Properties. *Eur. J. Org. Chem.* **2009**, 3535–3543.

(63) Capobianco, A.; Caruso, T.; Celentano, M.; La Rocca, M. V.; Peluso, A. Proton Transfer in Oxidized Adenosine Self-Aggregates. *J. Chem. Phys.* **2013**, *139*, 145101–4.

(64) Borrelli, R.; Di Donato, M.; Peluso, A. Role of Intramolecular Vibrations in Long-range Electron Transfer between Pheophytin and Ubiquinone in Bacterial Photosynthetic Reaction Centers. *Biophys. J.* **2005**, *89*, 830–841.

(65) Gieseking, R. L.; Risko, C.; Brédas, J.-L. Distinguishing the Effects of Bond-Length Alternation versus Bond-Order Alternation on the Nonlinear Optical Properties of π-Conjugated Chromophores. *J. Phys. Chem. Lett.* **2015**, *6*, 2158–2162.

(66) Jacquemin, D.; Adamo, C. Bond Length Alternation of Conjugated Oligomers: Wave Function and DFT Benchmarks. *J. Chem. Theory Comput.* **2011**, *7*, 369–376.

DOI: 10.1021/acs.jpca.6b05220

(67) Capobianco, A.; Velardo, A.; Peluso, A. DFT Predictions of the Oxidation Potential of Organic Dyes for Opto-Electronic Devices. *Comp. Theor. Chem.* **2015**, *1070*, 68–75.

(68) Jacquemin, D.; Zhao, Y.; Valero, R.; Adamo, C.; Ciofini, I.; Truhlar, D. G. Verdict: Time-Dependent Density Functional Theory “Not Guilty” of Large Errors for Cyanines. *J. Chem. Theory Comput.* **2012**, *8*, 1255–1259.

(69) Dierksen, M.; Grimme, S. Density Functional Calculations of the Vibronic Structure of Electronic Absorption Spectra. *J. Chem. Phys.* **2004**, *120*, 3544.

DOI: 10.1021/acs.jpca.6b05220

Graphical TOC Entry

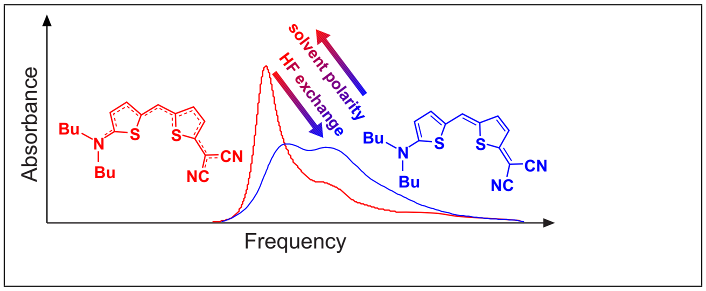

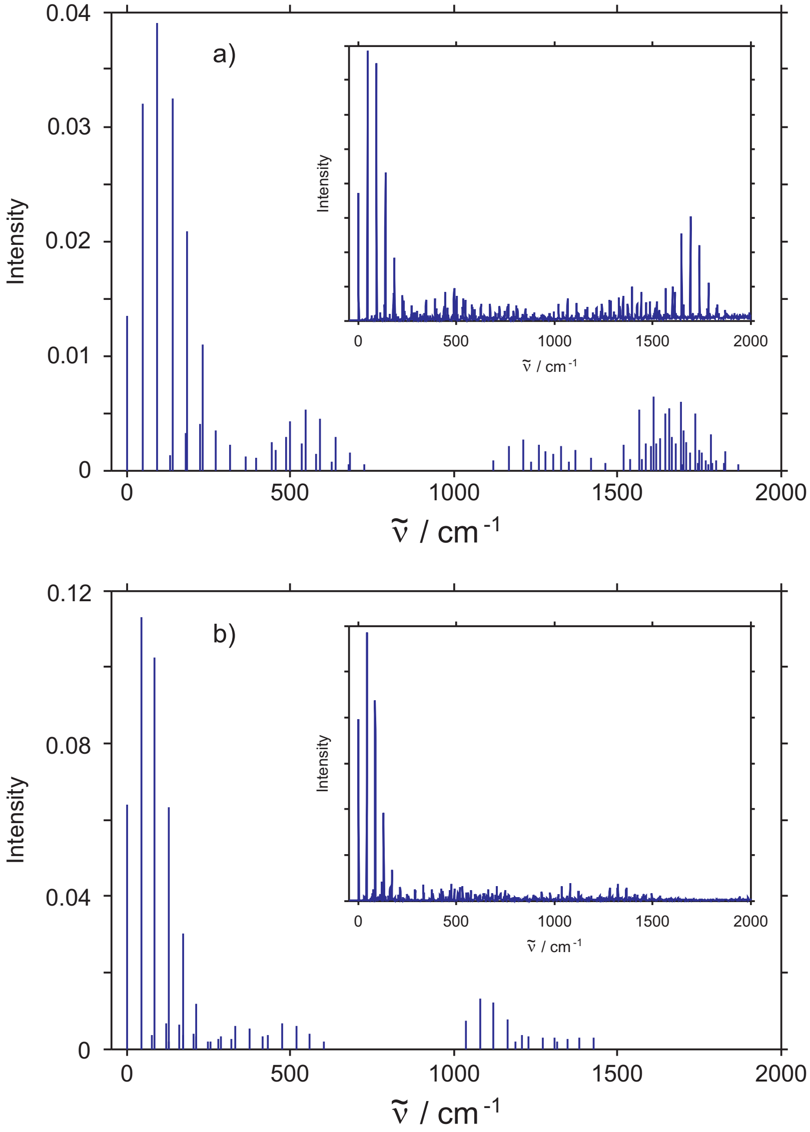

Figure 5: Computed CAM* a) and B3LYP b) absorption spectra of **1** at 0 K. Insets: absorption spectra predicted by the GF approach at 4 K.

Table 6: Ground state vibrational wavenumbers ($\tilde{\nu}_{\mathrm{gr}}$, cm^{-1}) and equilibrium position displacements (adimensional units) of the most displaced normal modes of cyanine 1 in gas phase and acetonitrile.

gas				AN			
B3LYP		CAM*		B3LYP		CAM*	
$\tilde{\nu}_{\mathrm{gr}}$	K	$\tilde{\nu}_{\mathrm{gr}}$	K	$\tilde{\nu}_{\mathrm{gr}}$	K	$\tilde{\nu}_{\mathrm{gr}}$	K
35	−0.22	32	−0.26	28	−0.12	44	1.72
41	1.92	33	0.13	38	−0.20	71	0.16
69	−0.19	44	2.25	41	1.54	88	0.29
82	0.16	68	−0.30	81	0.46	96	−0.18
89	0.34	95	−0.27	101	0.30	104	−0.33
95	0.14	147	−0.45	124	−0.26	126	−0.27
126	0.24	157	−0.12	243	−0.17	140	−0.26
146	−0.16	193	0.32	254	0.17	178	−0.11
186	−0.13	246	−0.25	283	0.40	291	0.40
241	−0.22	298	0.31	432	0.18	343	0.15
251	0.19	319	0.11	435	−0.23	443	0.11
287	0.31	343	−0.12	638	−0.11	457	−0.28
330	−0.15	440	0.41	681	−0.12	525	−0.10
422	0.25	453	−0.52	689	0.21	645	−0.11
436	−0.32	487	0.23	1076	0.35	725	0.27
468	0.12	508	−0.02	1182	0.16	730	−0.11
562	−0.15	518	0.11	1257	−0.12	1008	−0.13
606	−0.11	582	−0.29	1281	−0.13	1113	0.13
680	−0.18	625	−0.15	1392	−0.13	1221	−0.15
694	−0.18	701	0.21	1483	−0.16	1304	−0.15
1080	0.42	724	0.30			1326	−0.10
1109	−0.13	1010	−0.13			1369	0.18
1179	−0.24	1117	0.36			1620	0.10
1274	−0.20	1194	0.24			1694	0.41
1295	−0.17	1216	−0.34				
1351	−0.12	1270	0.25				
1399	−0.21	1326	0.07				
1489	0.14	1342	0.29				
1496	−0.18	1379	0.21				
		1467	0.18				
		1496	−0.18				
		1527	0.57				
		1533	0.27				
		1548	0.13				
		1576	−0.38				
		1627	0.29				
		1647	0.41				
		1673	0.56				
		1730	−0.17				
		2448	0.11				